Second harmonic generation as a probe of structure and dynamics of ionic liquids at the electrode interface

Naoya Nishi,* Hiromasa Baba, Takashi Yamazawa, Yuko Yokoyama, Tetsuo Sakka

Department of Energy and Hydrocarbon Chemistry, Kyoto University, Kyoto 615-8510, Japan

**Corresponding author: Naoya Nishi: nishi.naoya.7e@kyoto-u.ac.jp*

Abstract

Electrochemical second harmonic generation (ESHG) has been applied as a probe of the slow dynamics in the electric double layer (EDL) at the ionic liquid (IL)/Au interface. When the electrode potential was stepped, the SHG signal from the interface was relaxed on the time scale of longer than tens of seconds, which is distinctively slower than the *RC* time constant of the cell. This ultraslow relaxation in ESHG was quantitatively analyzed and discussed for several ILs, revealing that the ultraslow relaxation itself is a common phenomenon for the EDL in the ILs studied but the asymmetry of the time constants to the potential-step directions depends on the IL ions, which is likely to reflect the structure ordering of the interfacial ionic layer in the EDL depending on both ILs and the potential. The EDL structure in equilibrium has also been investigated via SHG measurements with a potential scan at a sufficiently slow rate; the potential dependence of the SHG signal was found to deviate from a simple parabolic one, reflecting the camel-shaped static differential capacitance for the EDL in ILs.

Keywords*: ionic liquid, surface plasmon resonance, differential capacitance, ionic multilayers, camel-shaped capacitance*

1. Introduction

Ionic liquids (ILs), which are salts composed of cations and anions with melting points lower than 100 °C, have several characteristics such as their liquid state over a wide temperature range and wide potential window. ILs have been extensively studied as electrolytes in electrochemical devices such as next-generation batteries and supercapacitors.[1–5] Since the electrode interface plays an important role in the electrode reactions and charging/discharging processes, it is indispensable to understand the structure and dynamics of the electric double layer (EDL) in ILs for their electrochemical applications.[6,7]

ILs are spontaneously structured at the interface,[8,9] forming a highly-viscous solid-like interfacial layer.[10–12] Previous studies using surface tension measurement,[13,14] electrochemistry,[15,16] x-ray reflectometry,[17–20] surface-enhanced infrared absorption spectroscopy,[21,22] and sum frequency generation[23,24] reported anomalously slow or even frozen structural relaxation of interfacial layer in ILs in response to potential perturbations. In our previous studies, we used electrochemical surface plasmon resonance (ESPR) to trace the ultraslow relaxation of the interfacial layer in ILs.[25–29] By using the SPR angle as a probe of the change in the local refractive index on the IL side of the IL/Au electrode interface, we found a two-step relaxation in ESPR; after a potential step, the SPR angle was immediately shifted to one direction, and then slowly relaxed to the other direction on the order of tens and hundreds of seconds, which is several orders of magnitude slower than the *RC* time constant of the cell. These two-step relaxations were ascribable to the polarization of IL ions in the interfacial layer. Among the several modes of polarization such as electronic, vibrational, orientational, and translational polarizations, the first SPR shift was proposed to attribute to the faster components other than translation, and the subsequent ultraslow relaxation was to the ionic translation, which is the charging process at the interface.[25,29]

In the present study, we investigate the ultraslow relaxation by focusing on the metal side of the IL/Au electrode interface with electrochemical second harmonic generation (ESHG),[30–34] a powerful technique to sensitively probe the charged state of the metal surface. SHG is a nonlinear optical phenomenon in which two photons with an angular frequency ω and a wavelength λ are converted to a single photon with 2ω and λ/2 via the interaction with a material. SHG has interfacial selectivity; SHG does not occur in the bulk phases if they have an inversion symmetry such as ILs and Au, and SHG signals are selectively generated only from the interfaces, where the inversion symmetry is broken, between such two bulk phases (as the IL/Au interface). While ESPR focuses on the IL side of the IL/Au electrode interface, ESHG focuses on the charged state of the Au electrode side of the IL/Au interface. Previous ESHG studies on the electrode interface of aqueous electrolyte solutions illustrated that the SHG intensity is parabolic with respect to the potential, with a minimum near the potential of zero charge (E_{pzc}).[30,35–41] This is due to an additional SHG term that is intensified with increasing the static electric field at the interface and becomes

comparable to and even dominant over the normal SHG term for the non-charged interface (see the Model section for details). ESHG has been applied to study the *RC* relaxation[42,43] and electrode reaction kinetics, such as electrodeposition[35,43–46] and adsorption,[36,40,47–51] at the electrode interface of aqueous electrolyte solutions. Non-aqueous electrolytes have also been studied with ESHG.[52] Since SHG has already revealed molecular-level structures at the non-electrochemical air[53–55] and water[53,54] interfaces of ILs, its application to the electrochemical interface of ILs is worth to be explored. Here, in the present study, we apply ESHG to the IL/electrode interface to investigate the ultraslow relaxation of the interfacial structure as well as to explore its potential dependent behavior. We will show that ESHG, which sensitively probes the electrode surface, can track the ultraslow relaxation like ESPR, but from a different aspect, the charged state of the electrode. The relaxation time constants for several ILs will be presented and discussed. Furthermore, we will also show that the potential dependence of SHG intensity deviates from the conventional parabolic behavior, stemming from the camel-shaped potential dependence of the static differential capacitance[56,57] of the EDL in ILs. We illustrate that ESHG is not only a relaxation probe but also a static capacitance probe.

2. Experimental

1-Butyl-3-methylimidazolium bis(trifluoromethanesulfonyl)amide (C_4mimTFSA) was prepared and purified according to the method in our previous studies.[58–60] Other three ILs, C_2mimTFSA,[57] TOMATFSA,[61,62] and C_2mimBF_4[63] were similarly prepared and measured to compare with C_4mimTFSA (C_2mim^+: 1-ethyl-3-methylimidazolium; $TOMA^+$: trioctylmethylammonium). The structures of these ions are shown in Fig.S1.

The ESHG setup is shown in Fig. S2. A spectroscopic electrochemical cell (EC FRONTIER) with a quartz window was used. The working electrode (WE) was a Au disk with a diameter of 3 mm, whose polycrystalline surface was polished to a mirror finish with aqueous slurries of alumina powders (0.05 μm) on a polishing cloth before each measurement. Pt wire and Ag/AgCl wire were used as the counter electrode (CE) and the quasi-reference electrode (QRE), respectively. ILs were injected into the cell in an argon-filled glove box after being evacuated using an oil pump for at least 2 h. The potential of WE with respect to QRE, denoted as *E*, was controlled with a potentiostat (SP-50, BioLogic). The potential-step SHG measurements (PS-ESHG) and linear-sweep SHG measurements (LS-ESHG) were performed within the polarized potential window (Fig.S3). A Ti:Sapphire laser (CPA2001, Clark-MXR) with a wavelength of 775 nm, pulse width of 150 fs, and repetition rate of 1 kHz, was used as the source of the fundamental (ω) beam. The ω beam was made p-polarized with a polarizer and focused with a lens at an angle of incidence of 60° to the cell (the angle of incidence at the C_4mimTFSA/Au interface was estimated

to be 38°). The beam power of ω light was 20 mW, and the beam energy density at the interface was 6 mJ cm^{-2}. The second harmonic (2ω) light generated before the sample was removed by a 2ω cut filter put just before the cell. The ω light reflected from the interface was cut by an ω-cut filter put just after the cell. The 2ω light generated from the interface was passed through a polarizer to be p-polarized, separated with a monochromator, and detected by a photomultiplier (R1527, Hamamatsu). The number of photons was counted with a photon counter (SR400, SRS). All measurements were performed at the room temperature controlled at 22 °C.

3. Model

The intensity of SHG light, $I_{2\omega}$, generated from the interface in the *p*-in *p*-out condition can be expressed as;[35,37]

$$I_{2\omega} \propto \left| \sum_{i,j,k}^{x,z} F_{ijk} \left(\chi_{ijk}^{(2)} E_{\omega} E_{\omega} + \chi_{ijkz}^{(3)} E_{\omega} E_{\omega} E_{\mathrm{dc}} \right) \right|^2 \tag{1}$$

where $\chi_{ijk}^{(2)}$ is the *ijk* component of the second-order susceptibility, $\chi_{ijkz}^{(3)}$ is the *ijkz* component of the third-order susceptibility, E_{ω} is the electric field of the fundamental light, E_{dc} is the dc (static) electric field at the interface that is along the surface normal, *z*, F_{ijk} ($= F_i^{2\omega} F_j^{\omega} F_k^{\omega}$) is the Fresnel factor, and *i*, *j*, and *k* are either of *x* or *z*, and the *x* and *z* axes are defined so that the incident and reflected light beams are in the *x*-*z* plane with the surface normal direction *z*. By merging the *ijk* susceptibility components and the Fresnel factors into one variable for each susceptibility term, we simplify eq 1 as,

$$I_{2\omega} \propto \left| \chi^{(2)} + \chi^{(3)} E_{\mathrm{dc}} \right|^2 I_{\omega}^2 \tag{2}$$

with

$$\chi^{(2)} = \sum_{i,j,k}^{x,z} F_{ijk}\, \chi_{ijk}^{(2)}$$

$$\chi^{(3)} = \sum_{i,j,k}^{x,z} F_{ijk}\, \chi_{ijkz}^{(3)} \tag{3}$$

For E_{dc}, we assume that the $\chi^{(3)}$ term is dominated by the Au electrode surface, not by the EDL region. Under this assumption, E_{dc} is simply connected with the surface charge density on the electrode, q_{M},

$$I_{2\omega} \propto \left|\chi^{(2)} + \chi^{(3)} \frac{q_{\mathrm{M}}}{\varepsilon\varepsilon_0}\right|^2 \tag{4}$$

where ε and ε_0 are the relative permittivity and the permittivity in vacuum, respectively. This assumption is justified by the fact that with the fundamental beam with 775 nm Au is in the 2ω resonant condition with the interband transition whereas IL ions studied are not in either ω or 2ω resonance. For q_{M}, we test two models to be fitted to experimental $I_{2\omega}$ vs. E data. One is the simple Helmholtz model (H model),

$$\frac{q_{\mathrm{M}}}{\varepsilon\varepsilon_0} = \frac{RT}{dF}\varphi \tag{5}$$

where R, T, and F are the gas constant, the absolute temperature (295 K), and the Faraday constant, respectively, d is the distance between the electrode surface and the Helmholtz plane, and φ, the dimensionless electrode potential, is

$$\varphi = \frac{F}{RT}\left(E - E_{\mathrm{pzc}}\right) \tag{6}$$

with E_{pzc} being the potential of zero charge. The H model can reproduce the parabolic potential dependence of $I_{2\omega}$ observed at the aqueous electrolyte solution/electrode interface.[30,35–41] The other is the mean-field lattice-gas model (LG model) for the EDL in ILs[56]

$$\frac{q_{\mathrm{M}}}{\varepsilon\varepsilon_0} = \frac{RT}{\kappa^{-1}F}\,\mathrm{sgn}(\varphi)\sqrt{\frac{2}{\gamma}\ln\{1 + 2\gamma\,\sinh^2(\varphi/2)\}} \tag{7}$$

where κ^{-1} is the Debye length, γ is the "compacity" parameter, and sgn() is the sign function. It should be noted that in the present study, unlike our previous ESPR study, we do not use another version of LG model[64] that includes a parameter for the local interionic electrostatic interaction, because the parameter was found to be unable to be assessed independently with γ in the ESHG analysis, unlike ESPR. In fitting with these two models, we used the following equation,

$$I_{2\omega} = B\left|1 + \left(Ae^{I\delta}\right)Q_{\mathrm{M}}\right|^2 \tag{8}$$

where B is a proportionality constant, $Ae^{I\delta}$ is the dimensionless complex ratio of $\chi^{(3)}$ on $\chi^{(2)}$ with A and δ being its absolute value and phase, respectively, and Q_{M} is the dimensionless surface charge density, written as:

$$Ae^{I\delta} = \frac{RT}{XF}\frac{\chi^{(3)}}{\chi^{(2)}} \tag{9}$$

$$Q_{\mathrm{M}} = \frac{XF}{RT}\frac{q_{\mathrm{M}}}{\varepsilon\varepsilon_0}$$

where X is d in the H model or κ^{-1} in the LG model.

The time constant of the relaxation of the interfacial structure against the potential switch was evaluated from PS-ESHG measurements. The time t variation of $I_{2\omega}$, $I_{\mathrm{P}\to\mathrm{N}}(t)$, when the potential was stepped from the positive to negative potential at $t = 0$, and vice versa, $I_{\mathrm{N}\to\mathrm{P}}(t)$, was simultaneously fitted with the following exponential decay functions.

$$I_{\mathrm{P}\to\mathrm{N}}(t) = I_{\mathrm{P}} + U(t)(I_{\mathrm{N}} - I_{\mathrm{P}})\left[\sum_{i=1}^{1\text{ or }2} f_{\mathrm{N}i}\{1 - \exp\left(-t/\tau_{\mathrm{N}i}\right)\}\right]$$
$$I_{\mathrm{N}\to\mathrm{P}}(t) = I_{\mathrm{N}} + U(t)(I_{\mathrm{P}} - I_{\mathrm{N}})\left[\sum_{i=1}^{1\text{ or }2} f_{\mathrm{P}i}\{1 - \exp\left(-t/\tau_{\mathrm{P}i}\right)\}\right] \quad (10)$$

where I_{P} and I_{N} are the SHG intensity in equilibrium, $\tau_{\mathrm{P}i}$ and $\tau_{\mathrm{N}i}$ are the i component of decay time constant, and $f_{\mathrm{P}i}$ and $f_{\mathrm{N}i}$ are the fraction of i component, all at the positive (P) and negative (N) potentials, respectively. $U(t)$ is the unit-step function. We tested the single and double exponential decay functions and adopted the latter only when its Corrected Akaike Information Criterion (AICc)[65] value was better (smaller) than the former's. For the latter case, the overall time constant τ was evaluated as the logarithmic mean:

$$\log\tau = f_1\log\tau_1 + (1 - f_1)\log\tau_2 \quad (11)$$

4. Results and discussion

4.1 PS-ESHG

To track the relaxation of interfacial structure in PS-ESHG measurements, SHG intensity was monitored during multi-potential-step perturbation between two potentials at the C_4mimTFSA/Au electrode interface. The potential was stepped between 0.0 V and −0.8 V at least five times repeatedly every 500 s, and the SHG data were averaged. The results for the negative and positive potential steps are shown in Figs. 1a and 1b, respectively. The SHG intensity varied in several seconds after the potential step at t = 0, and further relaxed to $I_{2\omega}$ in equilibrium at the post-step potential on the order of 100 s. Such a relaxation is several orders of magnitude slower than the *RC* time constant of the cell for C_4mimTFSA, 6 ms, which was estimated from the resistance R of 1.8 kΩ measured using electrochemical impedance spectroscopy and the capacitance C approximated to be the static differential capacitance ~50 μF cm^{-2} from ESPR[27,28] multiplied with the electrode surface area 0.070 cm^2. This ultraslow behavior has also been observed

in previous ESPR studies on the Au electrode interface of several ILs.[25,27,61] One can see that the relaxation against the positive direction (Fig.4b) is slower than the negative one (Fig.4a). This asymmetry with respect to the direction of potential perturbation, where the positive direction is slower, is also consistent with previous ESPR studies.[25,27,61] The SHG intensity in equilibrium at −0.8 V is lower than that at 0 V. This is qualitatively explained by the facts that −0.8 V is closer to −0.61 V, E_{pzc} of the C$_4$mimTFSA/Au interface,[27] and that the $\chi^{(3)}$ term of the ESHG is known to reach a minimum near E_{pzc}.[30,35–41] The potential dependence of SHG intensity will be discussed in detail below in the LS-ESHG section.

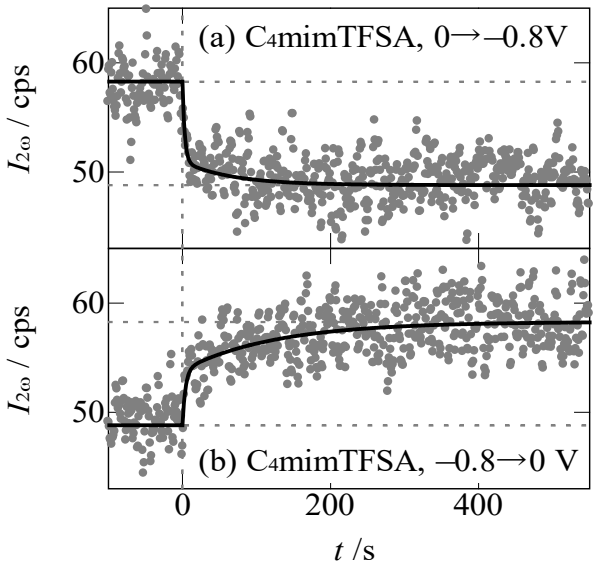

Figure 1. Time variation of SHG intensity for the C$_4$mimTFSA/Au interface in PS-ESHG. At t = 0 (vertical dashed lines) the potential was stepped (a) from 0 to −0.8 V and (b) from −0.8 to 0 V. The solid lines are from the fitting (eq 10). The horizontal dashed lines represent $I = I_{\mathrm{P}}$ and I_{N}.

For quantitative discussion, the PS-ESHG data were fitted by exponential functions (eq 10) and the relaxation time was evaluated. The black lines in Fig. 1 are the fitting results. The obtained fitting parameters are listed in Table S1, and the relaxation time constants are listed in Table 1. The relaxation time constants against the negative and positive potential steps, τ_{N} and τ_{P}, were estimated to be 6.2 s and 20 s, respectively (Table 1), which are several orders of magnitude slower than the *RC* time constant of the cell (6 ms). The ultraslow relaxation time constants qualitatively reproduce those by ESPR, which are also listed in Table 1. Regarding the asymmetry of τ toward the potential perturbation direction, $\tau_{\mathrm{P}}/\tau_{\mathrm{N}}$ is 3.2 for ESHG, greater than unity, indicating that the relaxation is slower for the positive direction (Table 1). This potential-direction asymmetry was also observed in ESPR, where $\tau_{\mathrm{P}}/\tau_{\mathrm{N}}$ is 140. More quantitatively, however, the τ values from ESHG and ESPR are different from each other; the τ_{N} of ESHG is an order of magnitude slower than that of ESPR whereas the τ_{P} in ESHG and ESPR is similar. There are

several possible reasons for this contrast. Firstly, the step potentials are different; the negative potentials are −0.8 V for ESHG in the present study but −1.2 V for ESPR, with the same positive potential of 0 V for them; ESHG investigates the interfacial structure at more positive potentials. In a previous ESPR study, we compared the step potential dependence of the asymmetry and found that more positive potentials result in less asymmetry, although the asymmetry itself kept appearing.[25] Secondly, what we detect is different; SHG detects the change in the charged state of the Au surface whereas ESPR probes the polarization relaxation of ions in EDL with a minor contribution of the Au surface.[29] Among several modes of polarization, fast ones such as electronic, vibrational, and orientational polarization more or less contribute to the ultraslow relaxation in ESPR, while ESHG will be much less sensitive to fast polarization and mainly detects the slowest translational polarization of ions, i.e., the charging process at the interface. This contrast between the behaviors of τ_N and τ_P in ESHG and ESPR illustrates the significant effect of the ionic species occupying the interfacial layer, anions at 0 V and cations at −0.8 V or −1.2 V, [28] on the polarization relaxation in EDL of ILs.

Table 1. Relaxation time evaluated from PS-ESHG and ESPR with the resistivity of ILs.

	τ /s (ESHG) [a]			τ /s (ESPR) [b]			ρ / Ω m [c]
	τ_N	τ_P	τ_P/τ_N	τ_N	τ_P	τ_P/τ_N	
C_4mimTFSA	6.2	20	3.2	0.34	49	140	3.1 [d]
C_2mimTFSA	7.8	47	6.0	-	-	-	1.3 [d]
TOMATFSA	11	38	3.5	1.2	23	19	220 [e]
C_2mimBF_4	12	3.7	0.31	-	-	-	0.88 [f]

[a] From potential step measurements between −0.8 and 0 V. [b] From potential step measurements between −1.2 and 0 V. [c] Bulk resistivity at 20 °C. [d] From ref.[66] [e] From ref.[67] [f] From ref.[68]

In our previous ESPR studies, we always obtained τ_P/τ_N greater than unity for the ILs investigated. All the ILs were based on amide anions like $TFSA^-$, although cations were relatively diverse: quaternary ammoniums or imidazoliums. To explore the similarity and dissimilarity of ESHG and ESPR, we further performed the PS-ESHG measurements on three other ILs, C_2mimTFSA, TOMATFSA, and C_2mimBF_4, which are composed of different cations and anions. The PS-ESHG results are shown in Fig. S4 and the best-fit parameters are listed in Table S1. The obtained relaxation time constants are listed in Table 1. All three ILs, like C_4mimTFSA, showed the ultraslow relaxation that cannot be explained by their *RC* time constants. Since the IL dependence of *C* is much smaller than that of *R*, the *RC* time constant can be approximated to be proportional to the bulk resistivity, ρ, of each ionic liquid. The resistivity is also listed in Table 1. There is no correlation between the relaxation time obtained with ESHG and resistivity (see also Fig.S5 for the plot). This is the same phenomenon observed for the IL dependence of ultraslow relaxation at the IL/W interface[14] and at the IL/Au interface,[61] confirming that the interfacial structure ordering rather

than the ionic mobility in the liquid bulk is a key factor to determine the structural relaxation of EDLs. Comparing τ_P/τ_N for the three $TFSA^-$-based ILs (C_4mimTFSA, C_2mimTFSA, and TOMATFSA), a similar degree of asymmetry, the slower relaxation in the positive direction, was observed, which is also similar to the ESPR for several amide-based ILs of TFSA,[27,61] bis(fluorosulfonyl)amide,[61] and bis(nonafluorobutanesulfonyl)amide.[25] On the other hand, for C_2mimBF_4 which is composed of a different anion, the asymmetry was rather opposite, with a slower relaxation in the negative direction. Since BF_4^- has a more symmetric ionic structure than $TFSA^-$, one would imagine that the interfacial layer structure at the positive potential occupied with anions is more ordered for the BF_4^--based IL, which presumably caused its greater τ_N than τ_P. From the asymmetry obtained with ESHG and ESPR, we propose that the interfacial structure ordering is in the order of BF_4^-, the cations, and amide ions from the highest.

4.1 LS-ESHG

To investigate the potential dependence of SHG intensity, linear sweep SHG measurements (LS-ESHG) were performed using C_4mimTFSA as an IL. The potential sweep direction was selected to be negative because of the smaller relaxation time constant ($\tau_N < \tau_P$, Table 1). The sweep rate, v, was chosen to be 0.25 mV/s, whose perturbation time constant RT/Fv = 100 s was sufficiently slower than τ_N, 6.2 s (Table 1). The potential was swept from 0.0 V to −1.2 V at a sweep rate of 0.25 mV/s, and the SHG intensity was measured simultaneously. After a sweep finished, the potential was immediately stepped back to 0.0 V and held there for 2400 s until the start of the next sweep to reset the interfacial structure (Fig. S6a). The results of sequential six measurements are shown in Fig. S6b, and the averaged results are shown in Fig. 2. The potential dependence of $I_{2\omega}$ is basically parabolic, as is known for the ESHG of the electrolyte solution/electrode interface.[30,35–41] ESHG is known to show a minimum $I_{2\omega}$ around E_{pzc}. The present SH intensity showed a minimum around −1.0 V, more negative than −0.61 V, E_{pzc} at the C_4mimTFSA/Au interface.[27] The negative shift of the SHG minimum potential from E_{pzc} agrees with a previous ESHG study at the Au electrode interface of aqueous electrolyte solutions using ω light with 1064 nm,[37] although both the shift amount and direction depend on the solid materials and the ω light wavelength.[37,41,69]

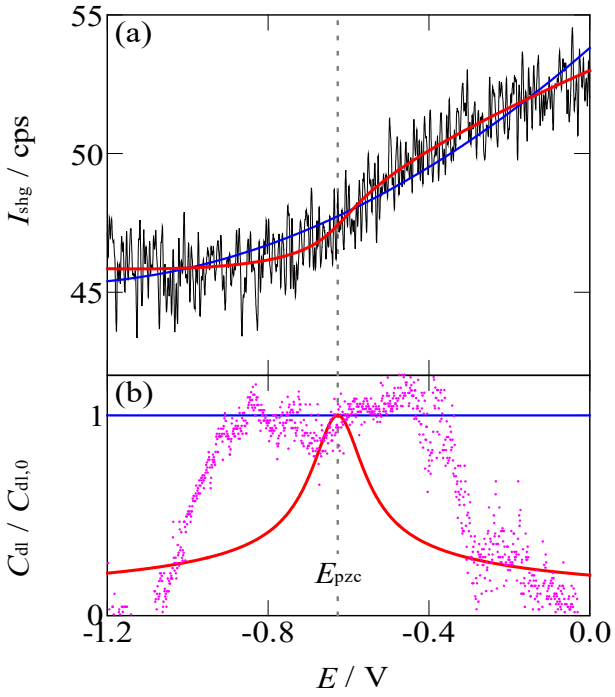

Figure 2. Potential dependence of (a) SHG intensity and (b) static differential capacitance at the C_4mimTFSA/Au interface from LS-ESHG. The blue and red lines are from the H and LG models, respectively. The vertical dashed lines are at E_{pzc}. The purple plots in (b) are from ESPR measurements.[27]

Regarding the parabola-like potential dependence of $I_{2\omega}$ shown in Fig.2a, its slope becomes slower on the far positive potential region −0.4~0 V. This implies that the H model on which the parabolic dependence is based cannot well describe the EDL in ILs. It has been reported theoretically[56] and experimentally[27,63] that the static differential capacitance for ILs decreases with increasing $|E - E_{pzc}|$, which is called camel-shaped behavior and different from either the flat one for the H model or the U-shaped one for the conventional Gouy-Chapman model. It should be noted that the *static* differential capacitance is the parameter to be compared and discussed between the theories and experiments, rather than the *non-static* one that is measurable by using electrochemical impedance spectroscopy, because the latter has strong frequency dependence and even dc-potential hysteresis. It is the static capacitance that influences the SHG intensity from the interface whose structure is in equilibrium. To clarify the potential-dependent capacitance behavior from ESHG, the fitting was performed using the H and LG models and the results are shown in Fig. 2a as blue and red lines, respectively. The best-fit parameters are listed in Table S2. One can see that the LG model well reproduces the LS-ESHG experimental results markedly better than the H model. Quantitative fitting results including AICc and the relative likelihood of the models can be found in Table S2. The values of log$A$ and δ, −1.66 and 79.5°, in the present study with 775 nm excitation conform with −0.16 and 25° at the Au interface of an aqueous electrolyte solution with 1064 nm excitation,[37] by taking account of the significant wavelength dependence of SHG response. The potential dependence of the static differential capacitance, evaluated from the

fitting results, is shown in Fig. 2b. One can see a camel-shaped behavior for the LG model (red line), where the capacitance decreases as the potential moves away from E_{pzc}, which is a common characteristic of EDLs in IL. The dependence is a one-hump camel shape rather than a two-hump one obtained with ESPR,[27] also plotted in Fig.2b. This discrepancy is likely to result from the relatively lower sensitivity of ESHG to the capacitance than ESPR; the $\chi^{(3)}$ term, which is the source to detect the potential dependence of the capacitance, is one order of magnitude smaller than the $\chi^{(2)}$ term, i.e., $\log A < -1$ (Table S2), in the present ESHG study whereas in ESPR the derivative of the SPR resonant angle with respect to the potential directly leads to the capacitance (multiplied by a proportional constant).[27] Nevertheless, a steep decrease in the static differential capacitance with increasing $|E - E_{\mathrm{pzc}}|$ was surely reproduced, similarly to the cases using electrocapillarity measured at the interfaces between liquid electrodes and ILs,[57,63,70] experimentally confirming the universality of this peculiar behavior of the static differential capacitance of EDL in ILs.

5. Conclusions

The present study successfully applied ESHG as a probe to track the ultraslow relaxation and the static differential capacitance of EDL in ILs. For the former, not only the ultraslow relaxation of EDL in ILs but also its asymmetry with respect to the potential perturbation direction was quantitatively analyzed at the Au electrode interface of several ILs by focusing on the charged state of the electrode. For the latter, a deviation from the simple parabolic potential dependence of the SHG signal was analyzed to extract the camel-shaped potential dependence of the static differential capacitance, a peculiar EDL behavior in ILs. Basically, it is difficult to evaluate the static differential capacitance at the solid electrode interface of ILs, however, ESHG is proven to be one of the methods such as ESPR.

In the future, a more comprehensive investigation of IL dependence would further reveal the EDL behavior in ILs, as partly shown in the present study. One of the other future directions is to use some electrode materials such as Ag, Pt, and Hg other than Au, as previously studied with ESHG for aqueous electrolyte solutions, because they are not in the 2ω resonance unlike Au and therefore SHG signal can be dominated with the $\chi^{(3)}$ term, which makes ESHG more sensitive to the EDL ultraslow relaxation and the static differential capacitance. However, without 2ω resonance of the electrode, it is possible to detect another SHG term originating from IL ions adsorbed on the electrode, which should have potential dependence different from $\chi^{(3)}$ and therefore may hamper the static differential capacitance measurements. On the other hand, such adsorption of ions on the electrode in "zero-solvent" ILs would be interesting to be pursued with ESHG.

Acknowledgements

This work was partly supported by the Japan Society for the Promotion of Science (JSPS) KAKENHI Grants (21H02046, 23H03829).

Author Declarations

Conflict of interest

The authors have no conflicts to disclose.

References

1. M. Watanabe, M.L. Thomas, S. Zhang, K. Ueno, T. Yasuda, K. Dokko, *Chem. Rev.* 117 (2017) 7190–7239.
2. X. Wang, M. Salari, D. en Jiang, J. Chapman Varela, B. Anasori, D.J. Wesolowski, S. Dai, M.W. Grinstaff, Y. Gogotsi, *Nat. Rev. Mater.* 5 (2020) 787–808.
3. N. Zhu, K. Zhang, F. Wu, Y. Bai, C. Wu, *Energy Mater. Adv.* 2021 (2021) 9204217.
4. O.M. Leung, T. Schoetz, T. Prodromakis, C. Ponce de Leon, *J. Electrochem. Soc.* 168 (2021) 056509.
5. K. Liu, Z. Wang, L. Shi, S. Jungsuttiwong, S. Yuan, *J. Energy Chem.* 59 (2021) 320–333.
6. D.S. Silvester, R. Jamil, S. Doblinger, Y. Zhang, R. Atkin, H. Li, *J. Phys. Chem. C*. 125 (2021) 13707–13720.
7. F. Chen, *Curr. Opin. Electrochem.* 35 (2022) 101086.
8. N. Nishi, Y. Yasui, T. Uruga, H. Tanida, T. Yamada, S.I. Nakayama, H. Matsuoka, T. Kakiuchi, *J. Chem. Phys.* 132 (2010) 164705.
9. J. Haddad, D. Pontoni, B.M. Murphy, S. Festersen, B. Runge, O.M. Magnussen, H.G. Steinrück, H. Reichert, B.M. Ocko, M. Deutsch, *Proc. Natl. Acad. Sci. U. S. A.* 115 (2018) E1100–E1107.
10. Y. Yokota, T. Harada, K.I. Fukui, *Chem. Commun.* 46 (2010) 8627–8629.
11. K. Ueno, M. Kasuya, M. Watanabe, M. Mizukami, K. Kurihara, *Phys. Chem. Chem. Phys.* 12 (2010) 4066–4071.
12. N. Nishi, T. Yamazawa, T. Sakka, H. Hotta, T. Ikeno, K. Hanaoka, H. Takahashi, *Langmuir*. 36 (2020) 10397–10403.
13. Y. Yasui, Y. Kitazumi, R. Ishimatsu, N. Nishi, T. Kakiuchi, *J. Phys. Chem. B*. 113 (2009) 3273–3276.
14. Y. Yasui, Y. Kitazumi, H. Mizunuma, N. Nishi, T. Kakiuchi, *Electrochem. Commun.* 12 (2010) 1479–1482.
15. S. Makino, Y. Kitazumi, N. Nishi, T. Kakiuchi, *Electrochem. Commun.* 13 (2011) 1365–1368.
16. T. Kakiuchi, Y. Yasui, Y. Kitazumi, N. Nishi, *ChemPhysChem*. 11 (2010) 2912 – 2918.
17. A. Uysal, H. Zhou, G. Feng, S.S. Lee, S. Li, P. Fenter, P.T. Cummings, P.F. Fulvio, S. Dai, J.K. McDonough, Y. Gogotsi, *J. Phys. Chem. C*. 118 (2014) 569–574.
18. R. Yamamoto, H. Morisaki, O. Sakata, H. Shimotani, H. Yuan, Y. Iwasa, T. Kimura, Y. Wakabayashi, *Appl. Phys. Lett.* 101 (2012) 130–133.
19. P. Reichert, K.S. Kjær, T. Brandt Van Driel, J. Mars, J.W. Ochsmann, D. Pontoni, M. Deutsch, M.M. Nielsen, M. Mezger, *Faraday Discuss.* 206 (2018) 141–157.
20. M. Chu, M. Miller, T. Douglas, P. Dutta, *J. Phys. Chem. C*. 121 (2017) 3841–3845.

21. K. Motobayashi, K. Minami, N. Nishi, T. Sakka, M. Osawa, *J. Phys. Chem. Lett.* 4 (2013) 3110–3114.
22. N. Nishi, K. Minami, K. Motobayashi, M. Osawa, T. Sakka, *J. Phys. Chem. C*. 121 (2017) 1658–1666.
23. W. Zhou, S. Inoue, T. Iwahashi, K. Kanai, K. Seki, T. Miyamae, D. Kim, Y. Katayama, Y. Ouchi, *Electrochem. Commun.* 12 (2010) 672–675.
24. W. Zhou, Y. Xu, Y. Ouchi, *ECS Trans.* 50 (2013) 339–348.
25. N. Nishi, Y. Hirano, T. Motokawa, T. Kakiuchi, *Phys. Chem. Chem. Phys.* 15 (2013) 11615–11619.
26. N. Nishi, Y. Ikeda, T. Sakka, *J. Electroanal. Chem.* 817 (2018) 210–216.
27. S. Zhang, N. Nishi, T. Sakka, *J. Chem. Phys.* 153 (2020) 044707.
28. S. Zhang, N. Nishi, S. Katakura, T. Sakka, *Phys. Chem. Chem. Phys.* 23 (2021) 13905–13917.
29. S. Zhang, T. Sakka, N. Nishi, *J. Electrochem. Soc.* 169 (2022) 066501.
30. C.H. Lee, R.K. Chang, N. Bloembergen, *Phys. Rev. Lett.* 18 (1967) 167–170.
31. G.L. Richmond, J.M. Robinson, V.L. Shannon, *Prog. Surf. Sci.* 28 (1988) 1–70.
32. R.M. Corn, D.A. Higgins, *Chem. Rev.* 94 (1994) 107–125.
33. B. Pettinger, C. Bilger, J. Lipkowski, SHG Studies on Halide Adsorption at Au(111) Electrodes, in: Solid—Liquid Interfaces, Springer Berlin Heidelberg, Berlin, Heidelberg, 2003: pp. 223–242.
34. Pierre-François Brevet, Surface Second Harmonic Generation, Presses Polytechniques Universitaires Romandes, 1996.
35. R.M. Corn, M. Romagnoli, M.D. Levenson, M.R. Philpott, *Chem. Phys. Lett.* 106 (1984) 30–35.
36. G.L. Richmond, *Chem. Phys. Lett.* 106 (1984) 26–29.
37. P. Guyot-Sionnest, A. Tadjeddine, *J. Chem. Phys.* 92 (1990) 734–738.
38. L. Werner, F. Marlow, W. Hill, U. Retter, *Chem. Phys. Lett.* 194 (1992) 39–44.
39. O.A. Aktsipetrov, A. V. Melnikov, T. V. Murzina, A.A. Nikulin, A.N. Rubtsov, *Surf. Sci.* 336 (1995) 225–231.
40. P. Galletto, S. Loridant, R. Antoine, P.F. Brevet, H.H. Girault, *J. Electroanal. Chem.* 500 (2001) 365–373.
41. P. Xu, A. Huang, J. Suntivich, *J. Phys. Chem. Lett.* 11 (2020) 8216–8221.
42. R.M. Corn, M. Romagnoli, M.D. Levenson, M.R. Philpott, *J. Chem. Phys.* 81 (1984) 4127–4132.
43. J.M. Robinson, G.L. Richmond, *Electrochim. Acta*. 34 (1989) 1639–1645.
44. T.E. Furtak, J. Miragliotta, G.M. Korenowski, *Phys. Rev. B*. 35 (1987) 2569–2572.
45. B. Pettinger, A. Friedrich, C. Shannon, *Electrochim. Acta*. 36 (1991) 1829–1833.
46. D.A. Koos, G.L. Richmond, *J. Phys. Chem.* 96 (1992) 3770–3775.
47. H.M. Rojhantalab, G.L. Richmond, *J. Phys. Chem.* 93 (1989) 3269–3275.
48. D.J. Campbell, R.M. Corn, *J. Phys. Chem.* 92 (1988) 5796–5800.
49. M. Buck, F. Eisert, J. Fischer, M. Grunze, F. Trager, *Appl. Phys. A Solids Surfaces*. 53 (1991) 552–556.
50. B. Pettinger, J. Lipkowski, S. Mirwald, A. Friedrich, *J. Electroanal. Chem.* 329 (1992) 289–311.
51. A.A. Tamburello-Luca, P. Hébert, P.F. Brevet, H.H. Girault, *J. Electroanal. Chem.* 409 (1996) 123–129.
52. H.T. Bian, Y. Guo, H.F. Wang, *Phys. Chem. Chem. Phys.* 20 (2018) 29539–29548.
53. N. Nishi, M. Yamamoto, T. Kakiuchi, *Bunseki Kagaku*. 56 (2007) 491–497.
54. N. Nishi, R. Ishimatsu, M. Yamamoto, T. Kakiuchi, *J. Phys. Chem. C*. 111 (2007) 12461–12466.
55. R. Costa, C.M. Pereira, A.F. Silva, P.F. Brevet, E. Benichou, *J. Phys. Chem. B*. 124 (2020) 3954–3961.
56. A.A. Kornyshev, *J. Phys. Chem. B*. 111 (2007) 5545–5557.
57. N. Nishi, S. Yasui, A. Hashimoto, T. Sakka, *J. Electroanal. Chem.* 789 (2017) 108–113.
58. K. Ezawa, N. Nishi, T. Sakka, *J. Electroanal. Chem.* 877 (2020) 114611.
59. N. Nishi, K. Ezawa, T. Sakka, *J. Electrochem. Soc.* 168 (2021) 072505.
60. S. Zhang, T. Yamazawa, T. Sakka, N. Nishi, *J. Phys. Chem. C*. 126 (2022) 9551–9558.
61. S. Zhang, H. Baba, T. Sakka, N. Nishi, *J. Electroanal. Chem.* 913 (2022) 116299.
62. N. Nishi, J. Uchiyashiki, R. Oogami, T. Sakka, *Thin Solid Films*. 571 (2014) 735–738.

63. N. Nishi, A. Hashimoto, E. Minami, T. Sakka, *Phys. Chem. Chem. Phys.* 17 (2015) 5219–5226.
64. Z.A.H. Goodwin, G. Feng, A.A. Kornyshev, *Electrochim. Acta*. 225 (2017) 190–197.
65. K.P. Burnham, D.R. Anderson, Model Selection and Multimodel Inference, 2nd Ed., Springer US, New York, 2002.
66. H. Tokuda, K. Hayamizu, K. Ishii, M.A.B.H. Susan, M. Watanabe, *J. Phys. Chem. B*. 109 (2005) 6103–6110.
67. L.M. Ramenskaya, E.P. Grishina, N.O. Kudryakova, *J. Mol. Liq.* 312 (2020) 113368.
68. A. Noda, K. Hayamizu, M. Watanabe, *J. Phys. Chem. B*. 105 (2001) 4603–4610.
69. E. Ma, P.E. Ohno, J. Kim, Y. Liu, E.H. Lozier, T.F. Miller, H.F. Wang, F.M. Geiger, *J. Phys. Chem. Lett.* 12 (2021) 5649–5659.
70. N. Nishi, Y. Kojima, S. Katakura, T. Sakka, *Electrochemistry*. 86 (2018) 38–41.